

PAPER

Research on mechanical properties of high-performance cable-in-conduit conductors with different design

To cite this article: Zichuan Guo *et al* 2020 *Supercond. Sci. Technol.* **33** 045002

View the [article online](#) for updates and enhancements.







IOP | ebooks™

Bringing together innovative digital publishing with leading authors from the global scientific community.

Start exploring the collection—download the first chapter of every title for free.

Research on mechanical properties of high-performance cable-in-conduit conductors with different design

Zichuan Guo^{1,2} , Chao Dai², Jinggang Qin² , Chao Zhou², Jiangang Li², Wu Yu², Fang Liu² , Dongsheng Yang², Chuanjun Huang³, Laifeng Li³, Hengcheng Zhang³, Tianjun Xue⁴, Arend Nijhuis⁵  and Arnaud Devred⁶

¹ University of Science and Technology of China, Hefei, Anhui, 230026, People's Republic of China

² Institute of Plasma Physics, Chinese Academy of Sciences, Hefei, Anhui, 230031, People's Republic of China

³ Technical Institute of Physics and Chemistry, Chinese Academy Sciences, Beijing, 100190, People's Republic of China

⁴ Baiyin Non-ferrous Changtong Wire & Cable Co., Ltd, Baiyin, Gansu, 730900, People's Republic of China

⁵ University of Twente, Energy, Materials and Systems, Faculty of Science and Technology, Enschede, 7500AE, Netherlands

⁶ CERN, TE Department, Geneva 23 1211, Switzerland

E-mail: dc@ipp.ac.cn (Chao Dai) and qinjj@ipp.ac.cn (Jinggang Qin)

Received 14 November 2019, revised 24 December 2019

Accepted for publication 22 January 2020

Published 17 February 2020



CrossMark

Abstract

The China Fusion Engineering Test Reactor (CFETR) is a new tokamak fusion reactor under preliminary design, where the toroidal field (TF) coil has been designed to create a magnetic field of over 14.3 T. The TF conductors need to operate stably at 14.3 T, requiring the exclusion of conductor performance degradation from thermal and electromagnetic loading as much as possible. The maximum Lorentz force will reach about 1200 kN m^{-1} , which is much higher than that of ITER conductors. In previous research, performance degradation was found during electromagnetic cycles and warm-up-cool-down cycles. A correlation was found between a conductor's degradation and its mechanical properties. According to the analysis, a conductor with a short twist pitch (STP) scheme or a copper wound superconducting strand (CWS) design has large stiffness, which enables significant performance improvement in terms of the electromagnetic and thermal load cycling. The cable stiffness is closely related to the number of inter-strand contact points inside the conductor. Based on this concept, four types of prototype cable-in-conduit conductor samples with STP and CWS design were manufactured. The number of inter-strand contact points was analyzed, and mechanical transverse load testing was performed at 77 K. The results show that the conductors with more contact points per unit length exhibit a higher stiffness. However, the cable designed with high cable stiffness caused strand indentation, which was also investigated. In this paper, the conductor design and experimental results are discussed and compared with ITER TF and central solenoid conductors.

Keywords: CFETR TF, CICC, conductor design, mechanical properties, strand contact points

(Some figures may appear in colour only in the online journal)

1. Introduction

The China Fusion Engineering Test Reactor CFETR is a new tokamak which is still under preliminary design [1]. The geometry and parameters of the magnetic field are calculated

according to the plasma burning control requirements. The CFETR magnet system consists of central solenoid (CS) coil modules, toroidal field (TF) coils, and poloidal field coils. The TF magnetic system is designed to keep the TF at a minimum ripple, and the peak magnetic field in the winding pack is kept

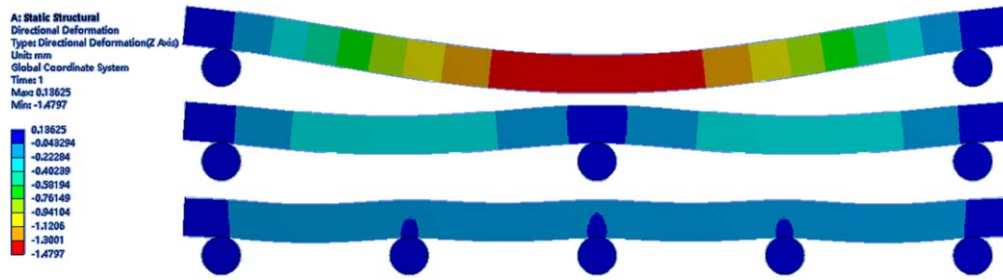


Figure 1. Typical example of the influence of the number of strand contact points per unit length. The strands are bearing the same pressure and contact with the other two, three, or five strands, and the Lorentz force and inter-strand contact are simplified for simulations. The regulation of real inter-strand contact can be described by this method.

below the maximum magnetic field constraints of the superconducting magnets. In the meantime, space is needed in the tokamak system to allow a tritium breeding rate of 1.2. According to the requirements, the maximum magnetic field in the TF winding pack will reach 14.3 T. The TF coil is foreseen to be made of cable-in-conduit conductors (CICCs). This operating environment subjects the conductors to a peak transverse Lorentz force of about 1200 kN m^{-1} , which is more challenging for the conductor design as compared to ITER CICCs.

In the preliminary design of the CFETR, the TF CICCs were designated to be made of Nb_3Sn cables, which is similar to the ITER conductors [2–4]. However, in the previous design of the ITER TF magnet system, the TF conductors were prone to substantial irreversible degradation upon cyclic electromagnetic and thermal loads [5]. For the CFETR TF coils, the requirements are higher than for the ITER TF and CS. As was found in previous research [6–8], modification of the cable pattern and void fraction could lead to significant improvements or even prevent degradation, which was first demonstrated with a prototype ITER TF Nb_3Sn CICC with long twist pitch design and smaller void fraction. Also, the Nb_3Sn ITER CS CICCs with the short twist pitch (STP) design show barely any degradation [9, 10]. After testing the mechanical properties, the higher transverse cable stiffness of the STP conductors was found to be the likely reason for the limited performance degradation. The cable stiffness shows significant correlation with the number of the strand-to-strand contact points per unit length inside the conductor, as figure 1 shows. In order to increase cable stiffness, the inter-strand contact length needs to be increased, as this provides more lateral support against bending [8, 11–13]. Lengths being equal, a strand in contact with five other strands shows less bending than one with three contact points and even less than one with two contact points, and this means that the length of the twist pitch affects the number of contact points between strands [8, 14]. A shorter twist pitch increases the periodicity of the number of contact points between strands. The higher speed of the spin cycle of strands in cable manufacturing increases the engagement of strands in a cable [15, 16].

Furthermore, the CICC with copper wound superconducting strand (CWS) design could also increase the number of contact points per unit length inside the conductor [17]; the principles of both designs are displayed in figure 2.

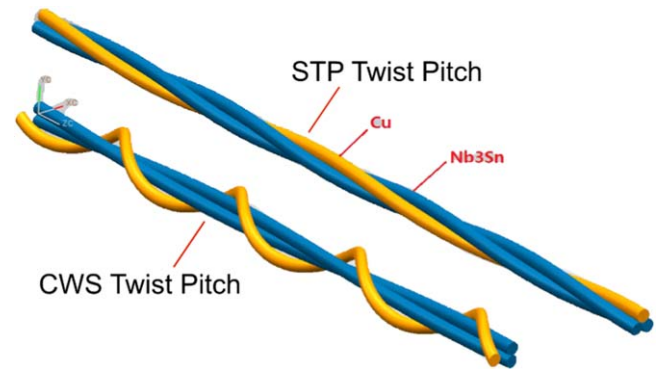


Figure 2. First stage cable with STP and CWS twist pitch designs.

In this paper, the mechanical properties and autopsies analysis of four different prototype conductors are discussed. Two of them (CFETR TF STP S01 (referred to as STP-S01) and CFETR TF STP S02 (STP-S02)) use the STP design, while the other two (CFETR TF CWS C01 (referred to as CWS-C01) and CFETR TF CWS C02 (CWS-C02)) use the CWS twist pitch method. Each STP and CWS sample was made with different lengths of twist pitch to compare the mechanical properties of different designs.

In order to simulate the Lorentz force, the CICCs are tested in a mechanical press machine. The cable stiffness is tested and compared within the same experimental environment and conditions. In the case of Lorentz force, the load is progressively accumulated over the conductor cross-section with a peak load of $I \times B$. The real electromagnetic load stress distribution inside the conductor cannot be simulated in the press. However, the samples' mechanical press test results can be analyzed by comparing the relationship between press test mechanical properties and electromagnetic cycle results, combined with the critical current decrease caused by the indentations of strands. After analyzing the mechanical press test properties of the TF conductor in detail, the CFETR TF conductor will be further optimized for cyclic electromagnetic testing in the SULTAN facility.

2. Conductor design

The CFETR TF CICC was designed with STP and CWS cable patterns separately, and assembled with a round-in-

Table 1. Parameters of the four CFETR TF samples.

| Item | STP-S01 | STP-S02 | CWS-C01 | CWS-C02 |
|----------------------------|----------|----------|--|--------------------|
| Strand diameter | | | 1.0 ± 0.005 mm | |
| Number of SC strands | | | 900 Nb ₃ Sn | |
| Number of Cu strands | | | 522 Cu | |
| Cable layout | | | [(2 SC + 1 Cu) × 3 × 5 × 5 + core] × 6 | |
| Stage 1 (2 SC + 1 Cu) [mm] | 30 ± 2 | 35 ± 3 | SC: 42 ± 3, Cu: 15 | SC: 50 ± 3, Cu: 20 |
| Stage 2 (× 3) [mm] | 65 ± 5 | 70 ± 5 | 70 ± 5 | 80 ± 5 |
| Stage 3 (× 5) [mm] | 90 ± 8 | 115 ± 8 | 100 ± 8 | 120 ± 8 |
| Stage 4 (× 5 + core) [mm] | 160 ± 15 | 190 ± 10 | 170 ± 15 | 190 ± 10 |
| Final Stage [mm] | 450 ± 20 | 450 ± 20 | 450 ± 20 | 450 ± 20 |
| Core layout | | | 3 × 4 | |
| Core pitch stage 1 (3 Cu) | | | 80 ± 5 mm | |
| Core pitch stage 2 (× 4) | | | 110 ± 10 mm | |
| Sub-wrap | | | 0.1 × 20 mm | |
| Coverage | | | 50% | |
| Wrap | | | 0.1 × 40 mm | |
| Overlap | | | 30%–40% | |
| Central spiral | | | 12.5 × 9.5 mm | |
| Cable diameter | | | 48.5 mm | |
| Conductor dimension | | | 65 mm | |
| Void fraction [%] | 32.1 | 32.6 | 31.2 | 31.6 |

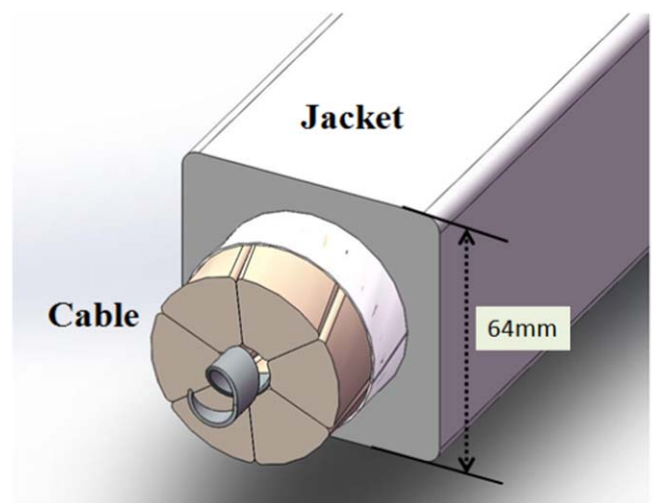
square jacket, as shown in figure 3. In order to match the compaction machine, a thin-wall round jacket was used, as shown in figure 4. A CFETR TF CICC contains 900 fully transposed superconducting (SC) strands, twisted up to five cabling stages. The final six sub-cable bundles are twisted around a central helical spacer that serves as a cooling channel. The cable is drawn into a circular stainless steel jacket and compressed into its required diameter and void fraction. According to the test condition requirements, the cable will be taken out of the original jacket after heat treatment. The cable outer diameter remained unchanged, which means that the thin jacket is strong enough to maintain the initial cable diameter during the heat treatment. Considering the samples only need to be pressed in the jacket with a vertical force, the effects of the thin jacket and the square jacket on the cable are the same.

The design parameters of the four samples are shown in table 1. The twist pitches of STP-S01 and CWS-C01 are shorter than those of STP-S02 and CWS-C02. In particular, the first stage copper (Cu) strand's twist pitch of CWS-C01 is shorter than that of CWS-C02.

The conductor cross-sections are shown in figure 4; each type of conductor was twisted with a different pitch. Thus, comparing the different designs could help to establish the relationship between mechanical properties and twist pitch.

3. Experimental methods

As the CFETR TF conductor was designed to operate under a maximum magnetic field of 14.3 T with a current of 87.6 kA, the electromagnetic load amounts to 1200 kN m⁻¹. In order to make a general judgment of the cable deformation, a cable

**Figure 3.** Preliminary design of the TF CICC.

mechanical press facility was built. For cable autopsies, a cable cross-section analysis method was established.

3.1. Strand contact points analysis

The cross-sections of 50 mm long conductor samples were polished and scanned to count the strand contact points. As illustrated in figure 5, the different first stage cables (triplets) were distinguished from each other using different colors. In the same first stage group, the SC strands are marked with hollow circles, and Cu strands are marked with solid circles. Because of the different manner of strand contact in the STP and CWS designs, the contacts in the first stage of STP cables are all in a state of line contact. Only point contact states between different first stages are counted in STP samples

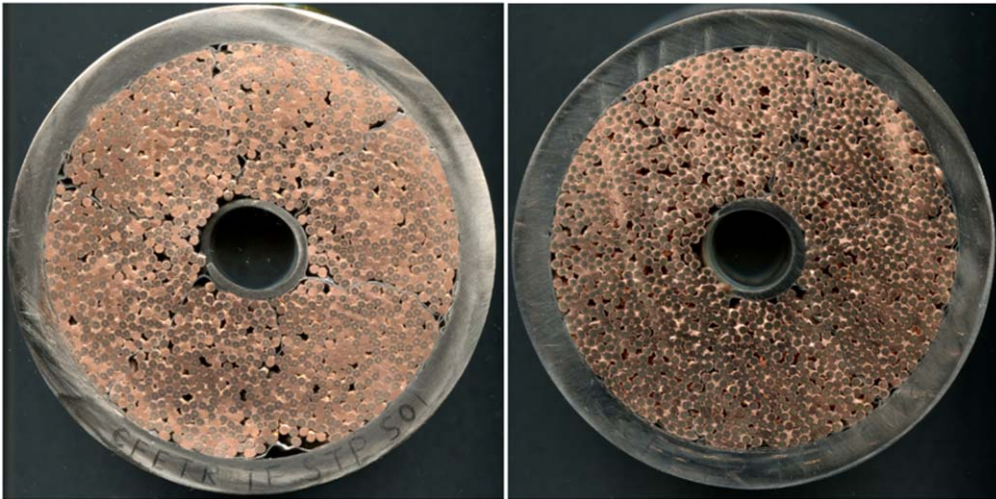


Figure 4. Cross-sections of the STP-S01 and CWS-C02 conductors.

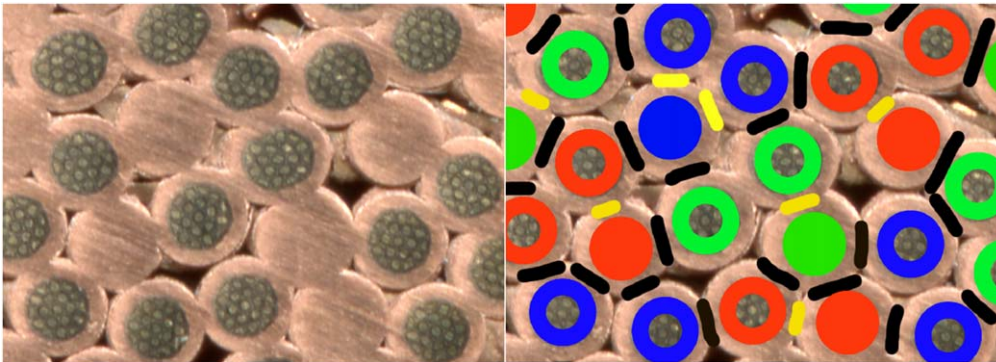


Figure 5. Part of the CFETR TF cable cross-section. The strands were classified as SC or Cu strands and as first cabling stage (triplet) or higher stage.

(marked with short black lines). The SC strands in the same first stage group of CWS cables are also in the line contact state, but contacts between Cu strands and SC strands are in the point contact state (marked with short yellow lines). For CWS samples, not only the contacts between different first stage cables are counted, but also the contacts between Cu strands and SC strands in the same first stage group.

3.2. Mechanical experiments

The four samples prepared for the cyclic loading test in the cryogenic press all went through a standardized preparation procedure, and the conductors were cut into 1000 mm and 550 mm length samples by spark erosion. The 1000 mm conductors were then dismantled to count the indentations of SC strands. The other conductors were heat treated according to the heat treatment scheme provided by the strand manufacturer. The conductors were then cut to 500 mm in length, and their jackets were split in half along the length by careful milling in order to allow cable compression under transverse load during the press test. The milling is done after both halves of the conductor's conduit are clamped by bolts to secure the initial void fraction. For the CFETR TF conductor samples, the circular jackets are dismantled, and the cable is

then installed into a conduit, which is circular inside and square outside to support and fit the sample in the press gap. Figure 6 shows a press sample fully prepared for measurement. This particular conduit was milled with computerized numerical control (CNC) machining technology in order to match the internal circle diameter with the outer cable diameter and secure the initial void fraction limitation. This method is known as 'limited void fraction' [18].

The mechanical testing machine is combined with the cable press unit for horizontal level debugging. The gap of the conduit is checked to ensure the same separation distance for every corresponding vertical position. The error in a horizontal mismatch is estimated to be lower than 10%. The displacement meter can be installed in any position to measure the displacement; in our case, it was installed on both sides of the gap. At the selected load cycles, the absolute displacement, representing the compaction of the cable, d , is measured, and the measurement was taken during the load–unload cycles. In every load–unload cycle the load goes from zero to maximum and then decreases to zero.

A schematic view of the cryogenic press is presented in figure 7. A hydraulic press drives the pillar at the top of the cryostat and transfers the force applied to the pressure

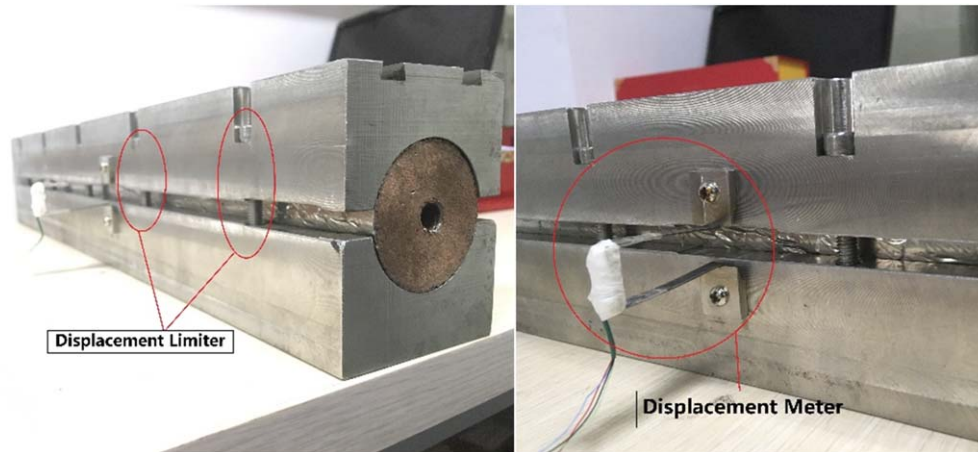


Figure 6. Displacement limiter and displacement meter installation locations.

dispersion module. The dispersion module transmits the force to Jacket-A of the conductor sample of length 500 mm, which is more than the length of the final stage twist pitch of the CFETR TF conductor. The strain gauges attached to the pillar of the press monitor the force applied to the sample, and together the displacement meters attached to the conductor allow the determination of the conductor's mechanical properties during load–unload cycles [19].

According to the designed operating requirement, the samples need to survive over 2000 electromagnetic cycles. In the mechanical cable press test, the sample undergoes the peak force 2000 times. The deformation of each conductor sample is recorded during the load–unload applied at cycle numbers 1, 2, 10, 100, 500, 1000, and 2000, from zero to full load state and back to zero. All the measurements were made during one cool-down session, and samples were continuously kept at 77 K in a liquid nitrogen bath.

After the cable mechanical press test, the samples were then measured in vertical and axial directions to confirm the cumulative plastic deformation. After the press measurements, the cables were then unraveled with extreme care in order to minimize any additional strain. Cable segments of about 10 mm in length were then cut using wire cutters, and polished. The primary purpose is to verify the difference between the cross-section change after the mechanical press and the electromagnetic cycle tests are done [20–23].

4. Experimental results

In this section, the results for CFETR TF conductors tested with the cable press are presented. Furthermore, analyses of the strand contact points from the conductor cross-sections and the strand indentations after press testing are presented.

4.1. Results of strand contact point counting

Four 50 mm long TF conductor sections were polished and scanned by a high-resolution scanner, allowing us to distinguish the SC from the Cu strands separately. Figure 8 gives an example of the scanning picture used to count the contact

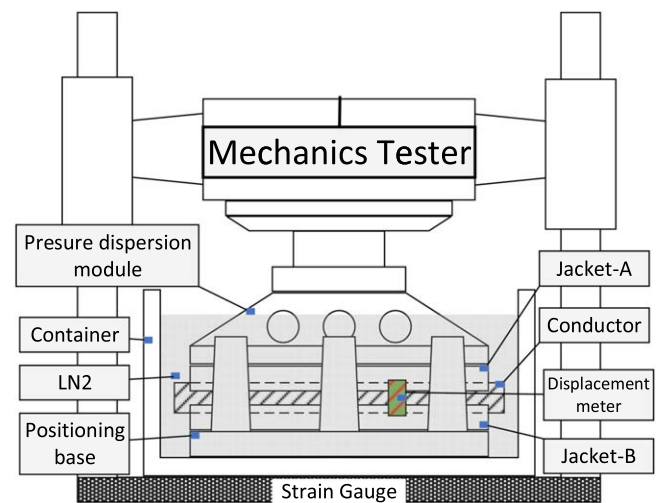


Figure 7. Schematic view of the cryogenic cable press.

points between the first stage cables before and after the mechanical press test.

As mentioned above, the statistics only account for the point contacts. For the first stage triplet of the STP cable, the contact between strands is in the line contact state, which means the strands are always in contact with each other, while in the CWS cable the twist pitch of the Cu strand is shorter than that of the SC strands, creating point contacts between Cu and SC strands. For this reason, the contact points between the Cu and SC strands in the first cable stage of the CWS were counted. The average of the contact points on the cross-section was calculated according to:

$$\text{Average of contact points} = \frac{\text{Count of contact points}}{\text{Cable cross-section area}} (\text{mm}^{-2}). \quad (1)$$

The strand contact point results are listed in table 2.

As shown in table 2, the STP and CWS-C02 samples show about an 8% decrease in the contact point distribution. Only the CWS-C01 sample shows an increasing rate of contact points compared to the cables before the press test. In the CWS-C01 sample, the higher cable stiffness indicates that

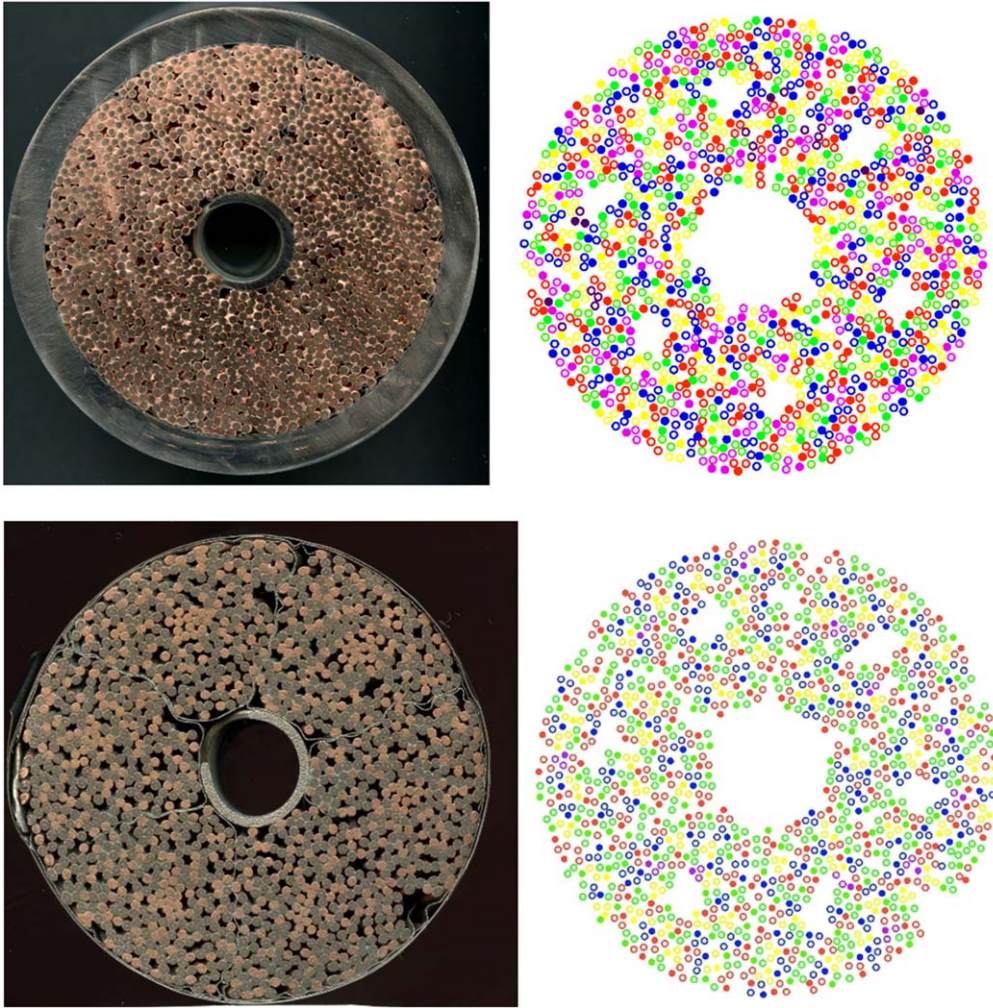


Figure 8. Example of strand contact point counting for the CWS-C02 conductor first stage cable. The different groups of the first stage cables are distinguished with different colors. The image of the cable with the jacket was scanned before cable press; the image of the cable without the jacket was scanned after cable press.

Table 2. Results of strand contact point counting from cable cross-section scanning.

| Item | STP-S01 | STP-S02 | CWS-C01 | CWS-C02 | ITER CS | ITER TF |
|--|---------|---------|---------|---------|---------|---------|
| Count of contact points (before press) | 1254 | 1148 | 2130 | 1994 | 665 | 582 |
| Average of contact points on cross-section (before press) [mm^{-2}] | 0.73 | 0.67 | 1.23 | 1.16 | 0.80 | 0.47 |
| Count of contact points (after press) | 1152 | 1060 | 2400 | 1820 | — | — |
| Average of contact points on cross-section (after press) [mm^{-2}] | 0.67 | 0.61 | 1.40 | 1.06 | — | — |
| Change ratio [%] | 8.13 | 7.67 | -12.67 | 8.73 | — | — |

the strands inside the cable might be compressed tighter, thus limiting the strand movement.

4.2. Results of cable press experiments

The CWS-C02 conductor is used as an example in figure 9, which shows a typical diagram of the cable deformation versus applied load with increasing number of cycles. The curves show a typical viscoelastic plastic deformation, which was observed earlier on CICC with apparent hysteresis behavior during the load-unload cyclic press test [24].

The other three samples show a similar deformation trend, but the maximum deformation is different. According to the displacement meter's recorded data, the maximum deformation, D_{max} , of the TF conductors is at the first full load cycle of the press. Figure 10 shows the maximum deformation of the four conductor samples compared to the results for the ITER TF and CS conductors measured at the University of Twente. According to [6, 19, 25], performance degradation has not been found in the ITER CS STP conductor but was found in the ITER TF with electromagnetic cycle test. Part of the relationship between a cable's mechanical properties and its

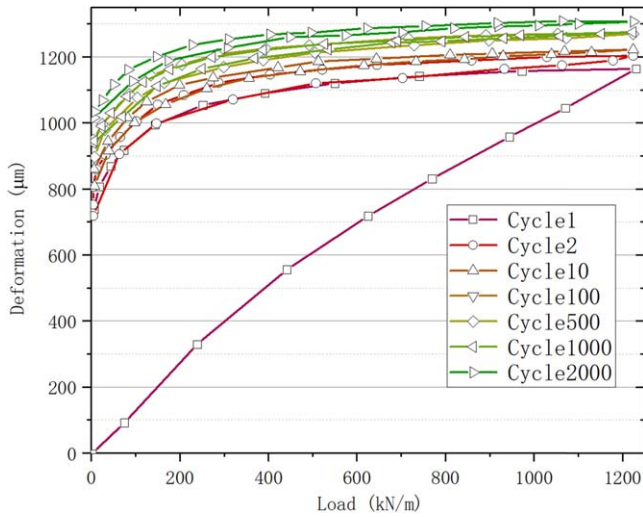


Figure 9. Example of typical deformation versus load curves for different numbers of cycles for the CWS-C02 sample.

electromagnetic performance can be established. The samples labeled JAS-JA and OST-EU are ITER TF conductors. The samples referred to as CS-JAS and CS-KAT are ITER CS conductor samples, and the sample marked CFETR-CSMC is a sample of the CFETR central solenoid model coil [19]. The trends of deformation with cycles are comparable to each other. In the first ten cycles, the D_{max} of the four samples shows the highest rate of deformation. The D_{max} of STP-S02 is $2182 \mu\text{m}$ in the 2000th cycle and shows the most considerable deformation of all conductor samples during the cyclic test. The CWS-C01 sample shows the least deformation, with D_{max} equaling $1232 \mu\text{m}$ at the 2000th cycle. It can be noted that the D_{max} of both CWS samples is less than that of the STP type.

Figure 11 shows the minimum cumulative deformation, which represents the plastic deformation of the TF conductors when the force was released entirely. The plastic deformation is irreversible, which could also alter the helium flow resistance. As shown, after 2000 cycles, the plastic deformation of the CWS-C01 sample displays the highest value at $911 \mu\text{m}$. The STP-S01 sample shows the lowest plastic deformation at $529 \mu\text{m}$. Both CWS-type conductors show substantially more plastic deformation than the STP-type conductors.

The elastic modulus is a parameter to evaluate the stiffness of a conductor. From figure 12, the effective elastic modulus of the conductor's transverse direction is calculated by the load–deformation data according to:

$$E_y = \frac{D \cdot F_y}{A_y \cdot d_y} \text{ (Pa)}, \quad (2)$$

where D is the conductor diameter, A_y (m^2) is the average longitudinal cable cross-section (projected cable area), and d_y is the absolute conductor deformation relative to its initial contour [24].

The evolutions of the samples' elastic moduli at maximum load as a function of number of cycles are compared in figure 13. Except for the E_{y-max} of the STP-S02 sample, which is lower than that of the ITER CS-JAS conductor, the other three samples all have a higher E_{y-max} than CS-JAS.

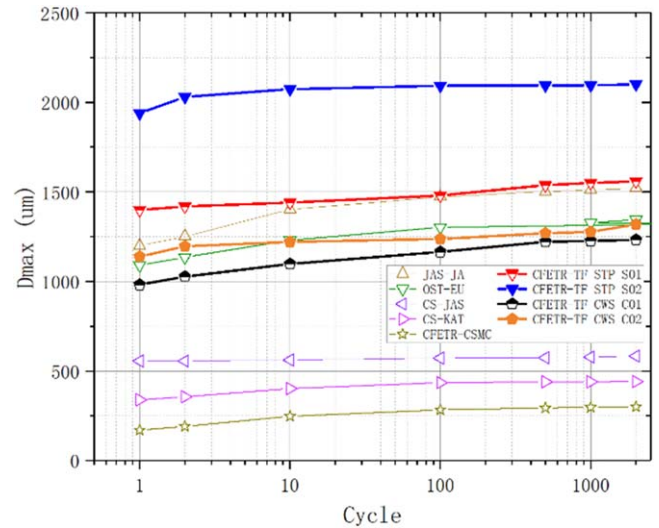


Figure 10. Maximum deformation (D_{max}) at 1200 kN m^{-1} load versus the number of load cycles of the CFETR TF conductors compared to results for the ITER TF and CS, and the CFETR-CSMC, conductors.

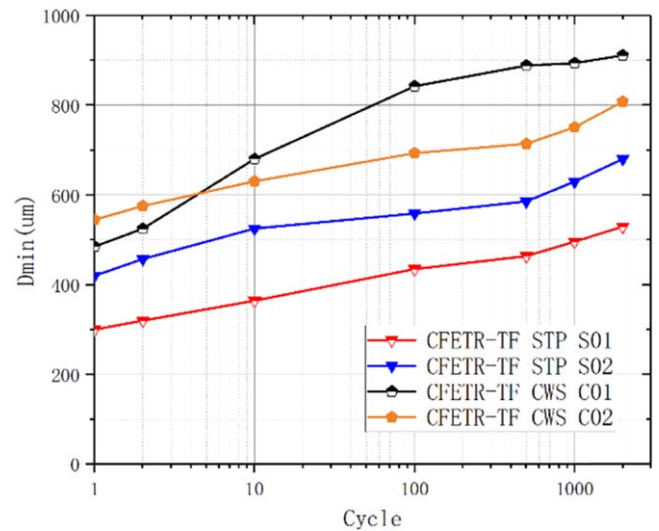


Figure 11. Minimum cumulative deformation (D_{min}) versus the number of cycles representing the plastic deformation when the sample was unloaded to zero.

The mechanical loss Q_m is the energy accumulation caused by strand contact surface friction and deformation under transversal load. The mechanical loss accumulated by a full load cycle is calculated as follows:

$$Q_m = \oint F_y \cdot d_y \text{ (J/cycle)}, \quad (3)$$

in which F_y is the load value in a cycle, and d_y is the displacement difference corresponding to the load [19].

As shown in figure 14, the mechanical loss of the four CFETR TF conductors is an order of magnitude higher than that of all other samples. The mechanical losses of different cables, as described, aims to show the trends of the mechanical losses of different cables. It also shows the higher

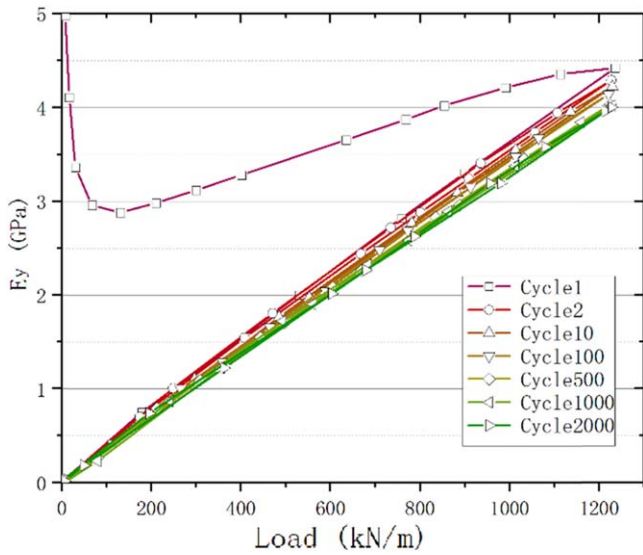


Figure 12. Example of typical elastic modulus versus load curves for different numbers of cycles of the CWS-C02 sample.

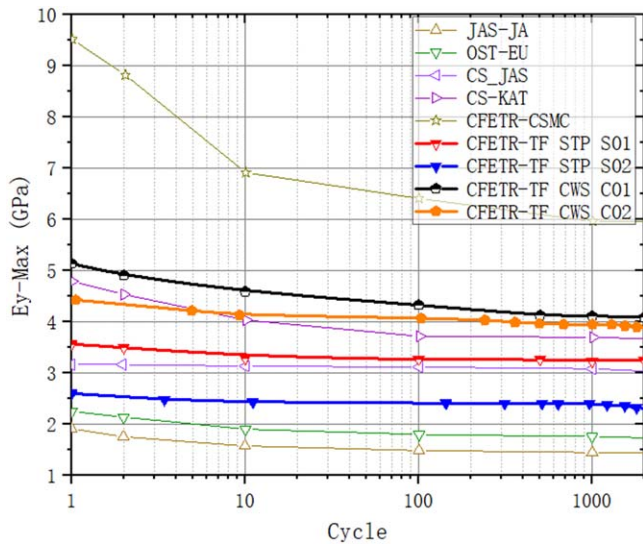


Figure 13. Evolution of the elastic modulus at maximum load (E_{y-max}) as a function of cycle number.

energy losses in the four samples compared to the other cables. By adding the ITER cables' results, the magnitude of the mechanical losses can be compared. Furthermore, this will be a reference dataset when establishing the relationship between the mechanical test and the electromagnetic test with a summary of the Pearson correlation coefficient. The Q_m of the CWS conductor samples is a little bit lower than that of the STP conductors. For all samples, the mechanical loss is quickly reduced by 80% at the first ten load cycles compared with the initial mechanical loss.

4.3. Statistics of unraveled strand indentations

As known from [14, 15, 17, 26, 27], the depth of indentations, which means the deformation damage of strands, can affect

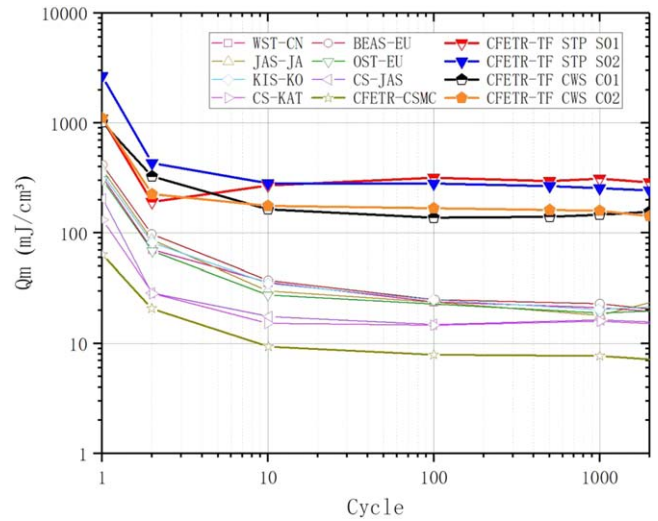


Figure 14. Evolution of the mechanical loss per load cycle versus the number of load cycles.

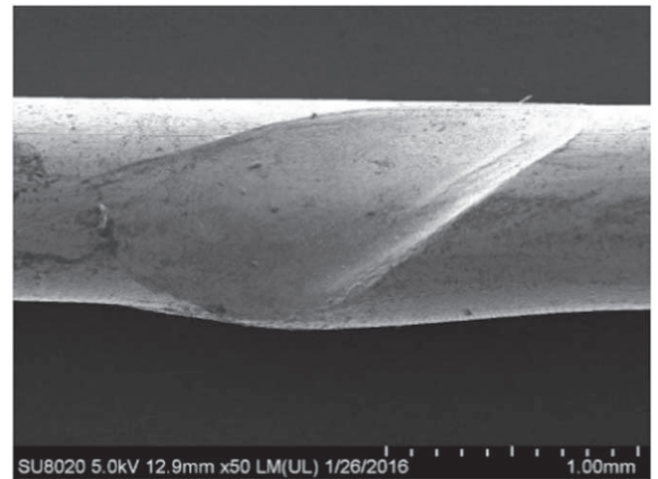


Figure 15. Example of a typical strand indentation caused by the cable manufacturing process.

the performance in terms of critical current (I_c) and residual resistivity ratio (RRR). A typical indentation of a strand is shown in figure 15.

Conductor sections of length 1 m are used for strand indentation measurement and counting. After unraveling the cable, the strands' indentations were measured one by one, before heat treatment. The strand indentation results are summarized in figure 16. For the STP conductors, the SC strand indentations in STP-S01 are systematically deeper than in STP-S02. For the CWS conductors, the indentations of CWS-C01 are higher than those of CWS-C02. Overall, the CWS-type conductors show more and deeper indentations than the STP-type.

The results listed in [26] show I_c -indentation results of a Nb_3Sn strand with a diameter of 0.82 mm. The acceptance criterion of indentation depth is less than 0.23 mm. If the strand diameter is scaled up to 1.0 mm, it should be less than

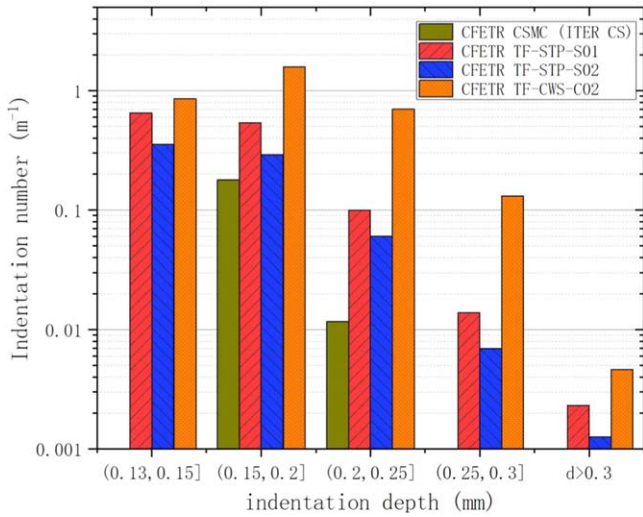


Figure 16. Counts of SC strand indentations per unit length versus indentation depth.

0.28 mm theoretically. The four conductor samples were manufactured with short strands, which are manufactured with billet. It is not representative to perform the I_c testing with indentation. Hence, the present acceptance criteria were set as 0.28 mm. In future, it will be updated with standard strand tests.

During the unraveling of strands for the indentation statistics, strand fractures were found in strands of the CWS-C01 cable, which could have been caused by the high compaction load during cable manufacturing. Examples of fractures shown in figure 17 are presumed to occur in the conductor manufacturing process. In the next phase, the twisting method of the CWS design will be reconsidered to avoid strand fractures.

5. Discussion

The results of the mechanical press tests, conductor cross-section, strand contact point analysis, and strand indentation evaluation are further specified and listed in table 3. To facilitate the presentation and comparison of the data, the titles of each group are replaced with [a], [b], [c], [d], [e], [f], [g], [h] and [i]. The further calculation of these results aims to express the process change of the cable's mechanical properties intuitively.

The results to be compared were normalized; the minimum values of every group were normalized to 1, and others were calculated proportionally. All the results were used to compare and establish the relationship between the cable's structural design and its performance. The results are shown in figure 18. The conductors were sorted by stiffness from high to low.

As shown in figure 16, the sample with CWS design shows more and deeper indentations, which could reduce further strand deformation and movement, further contributing to the stiffness of conductors as compared to those of the



Figure 17. Strand fractures found in the CWS-C01 sample.

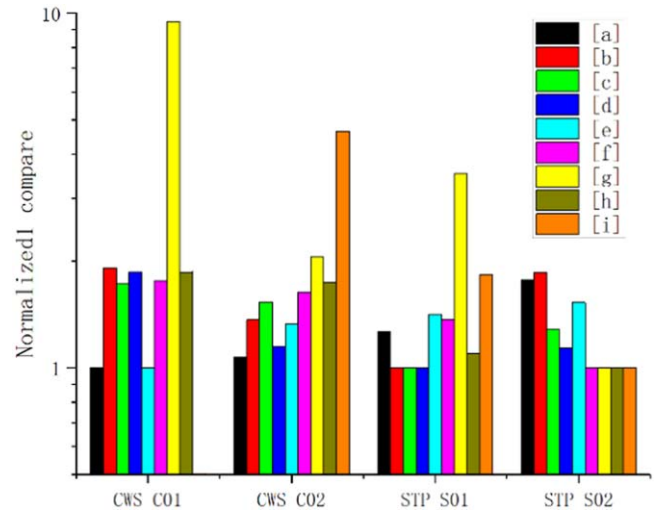


Figure 18. Comparison of TF conductors' test results.

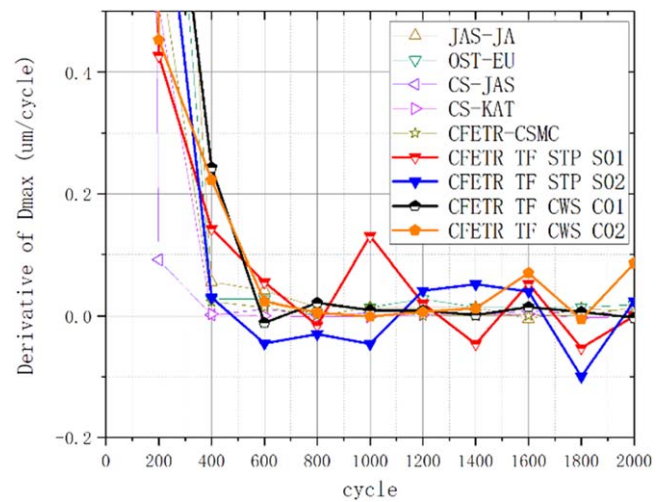


Figure 19. The derivative of D_{max} .

STP design. The change rate of the maximum deformation of the samples is displayed in figure 19. As shown, the derivative of D_{max} was calculated, and the values all quickly decreased to lower than 0.1 μm per cycle. The deformation rates of the four samples show similar trends and values compared with that of the ITER CS cable after 1000 load cycles. From this result, the maximum cable deformation is

Table 3. Further processing of experimental results.

| Item | STP-S01 | STP-S02 | CWS-C01 | CWS-C02 |
|---|---------|---------|---------|---------|
| [a] = $D_{\max-2000\text{cycle}}/D_{\text{TF cable initial diameter}}$ [%] | 3.21 | 4.50 | 2.54 | 2.72 |
| [b] = $(D_{\max-2000\text{cycle}}-D_{\max-1\text{cycle}})/D_{\max-1\text{cycle}}$ [%] | 6.55 | 12.2 | 12.5 | 8.93 |
| [c] = $D_{\min-2000\text{cycle}}/D_{\text{TF cable initial diameter}}$ [%] | 1.09 | 1.40 | 1.88 | 1.67 |
| [d] = $(D_{\min-2000\text{cycle}}-D_{\min-1\text{cycle}})/D_{\min-1\text{cycle}}$ [%] | 11.5 | 13.0 | 21.3 | 13.1 |
| [e] = $(D_{\max-2000\text{cycle}}-D_{\min-2000\text{cycle}})/(D_{\max-1\text{cycle}}-D_{\min-1\text{cycle}})$ [%] | 91 | 99 | 65 | 86 |
| [f] = Average of $E_{y\ 1\text{cycle}-2000\text{cycle}}$ [GPa] | 3.26 | 2.39 | 4.20 | 3.91 |
| [g] = Variance of $E_{y\ 1\text{cycle}-2000\text{cycle}}$ [%] | 0.60 | 0.17 | 1.61 | 0.35 |
| [h] = Average contact points on conductor cross-section [m^{-2}] | 0.70 | 0.64 | 1.31 | 1.10 |
| [i] = Average count of SC strand indentations [m^{-1}] | 1.30 | 0.71 | — | 3.30 |

[a] is the ratio of the final displacement of the cable to the initial conductor diameter;

[b] is the increasing rate of D_{\max} over 2000 cycles compared to D_{\max} of the first cycle;

[c] is the ratio of the plastic deformation of the cable to the initial conductor diameter;

[d] is the increasing rate of D_{\min} over 2000 cycles compared to D_{\min} of the first cycle;

[e] is the difference between maximum deformation and plastic deformation changing the ratio between the 2000th and first cycles;

[f] is the average of the elastic modulus from one to 2000 cycles;

[g] is the variance of the elastic modulus from one to 2000 cycles;

[h] is the average of the contact point count on the cable cross-section;

[i] is the average count of SC strand indentations.

considered to stabilize towards 2000 cycles. However, figures 9 and 10 indicate that the plastic deformation of the cables continues up to at least 2000 cycles.

The plastic deformation is mostly coming from the Cu strands' deformation, which might not cause the SC strands to strain intensely. Hence the plastic deformation seems to have less of an effect on the maximum cable deformation. Combined with previous studies [5, 6, 19], the maximum deformation shows more similarity with the electromagnetic cycle performance degradation. The stiffness of the STP-S01 sample is higher than that of the STP-S02 sample, because of the shorter twist pitch of STP-S01. The twist pitch of the CWS-C02 cable is longer than that of STP-S02, except for the Cu strands in the first stage. But it shows higher stiffness than STP-S02, which could be caused by the more considerable cable manufacture deformation of the Cu and SC strands in the CWS samples.

Considering that the cable stiffness of some of the samples has reached higher levels than that of the ITER CS, and that the trends of cable stiffness remain stable over later cycles, similar to ITER CS cable mechanical press and electromagnetic test results, the performance of CFETR TF samples is predicted to be able to maintain performance stability during electromagnetic cycling testing.

According to the cable deformation results, the maximum deformation of the CWS-C01 and CWS-C02 samples both show lower deformation during press testing than do the STP conductors. The CWS structural design can increase the cable stiffness, which is mostly caused by way of copper wire twisting, but at the same time it goes along with more severe cable manufacture deformation in terms of strand indentation.

In order to find out the impact of different cable twist stages on cable stiffness and strand contact points, a relevance test was established. With this method, the change of a structural parameter can be compared, and the impact can be analyzed. The Pearson correlation coefficient is calculated

using the following method:

$$\rho_{xy} = \frac{\text{cov}(X, Y)}{\sqrt{D(x)}\sqrt{D(Y)}}, \quad (4)$$

in which X, Y is the sample matrix, and each sample matrix consists of a single typical structural parameter of different samples. $\text{cov}(X, Y)$ is the covariance of X and Y , $D(x)$ is the variance of X , and $D(Y)$ is the variance of Y . The Pearson correlation coefficient is used to compare the correlation between the two dependent sets of data [28].

In this research, the contact points and elastic modulus are the feedback of the structural parameters, and the contact point results are set as one set of data to form the two sets of data with every stage of strand twist pitch parameter separately. The same method is used on the elastic modulus results. The value of the coefficient range is from -1 to 1 , and the higher absolute value of the Pearson correlation means the two sets of data are closed or affected. If the value is zero, this means the two sets of data are independent.

As shown in table 4, all results were used to compare and establish the relationship between the mechanical properties and conductor design. The first stage Cu strands show higher absolute value (0.971) than the SC strands (0.634), which means they play a more important role than the SC strands do in supporting the cable stiffness. Due to the negative sign of the value, a negative correlation between the first stage Cu strands' twist pitch length and the elastic modulus is established: the more extended the twist pitch of the first stage Cu strands, the lower the cable elastic modulus and stiffness.

The second stage plays a secondary role. The relevance of the strand contact points and elastic modulus is 0.932, which means the inter-strand contact points have a positive effect on elastic modulus, with more contact points resulting in higher elastic modulus and higher cable stiffness. The amount of strand contact points in CWS-C01 is 6.5% higher than in CWS-C02, and it is 7.4% stiffer than CWS-C02. The contact point count per unit length of STP-S01 is 9.7% higher

Table 4. Pearson correlation coefficient between cable twist stage, contact points, elastic modulus, and other results.

| Item | 1st stage SC | 1st stage Cu | 2nd stage | 3rd stage | 4th stage | Contact points | E_y |
|------|--------------|--------------|-----------|-----------|-----------|----------------|--------|
| [a] | -0.546 | 0.910 | -0.303 | 0.239 | 0.377 | -0.983 | -0.854 |
| [b] | 0.242 | -0.192 | 0.118 | 0.384 | 0.437 | -0.043 | 0.251 |
| [c] | 0.795 | -0.822 | 0.573 | 0.407 | 0.338 | 0.665 | 0.879 |
| [d] | 0.326 | -0.748 | -0.001 | -0.142 | -0.174 | 0.619 | 0.704 |
| [e] | -0.420 | 0.918 | -0.078 | 0.273 | 0.356 | -0.872 | -0.850 |
| [f] | 0.634 | -0.971 | 0.370 | -0.137 | -0.271 | 1.000 | 0.932 |
| [g] | 0.114 | -0.747 | -0.240 | -0.509 | -0.556 | 0.711 | 0.638 |
| [h] | 0.827 | -0.983 | 0.584 | 0.182 | 0.059 | 0.932 | 1.000 |
| [i] | 0.895 | -0.993 | 0.851 | 0.445 | 0.300 | 0.926 | 0.995 |

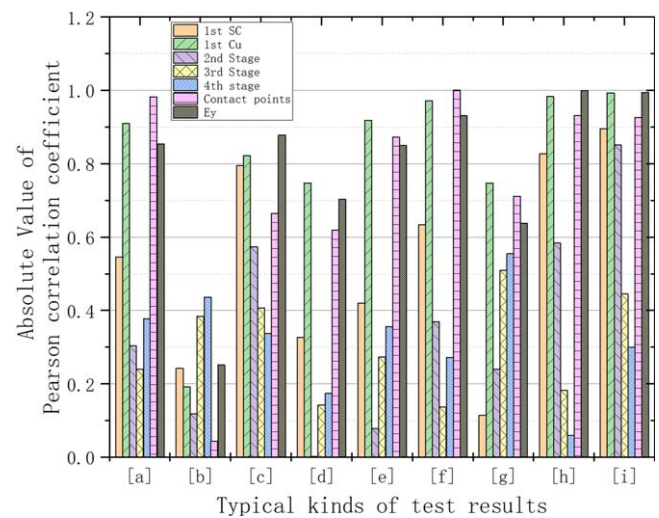
than that of STP-S02, and the cable is 37% stiffer. This shows that the number of contact points per unit length plays an essential role when the contact point density is relatively low, but the impact decreases when the contact point density exceeds a certain level. The material properties and strand diameter determine the specific level of contact points. On the other hand, it can be noted that the applied analysis method of counting the number of contacts does not account for the influence of line contact in the STP triplets.

In table 4 and figure 18, it can be found that the sample with higher stiffness (higher E_y) shows a more significant number of strand contact points per unit length. At the same time, the conductor deformation and the difference between D_{\max} and D_{\min} are smaller for higher stiffness. The CWS-type conductor samples are stiffer than those with STP design. They show a smaller difference between D_{\max} and D_{\min} than the STP samples, together with a lower void fraction. This lower void fraction means more restricted limitations for strand movements inside the conductor. Although the stiffness is higher, the CWS conductor samples were observed to have more severe indentations on the SC strands, and a more significant cable compression after load release, which might cause conductor performance degradation.

As shown in figure 20, the absolute value of the Pearson correlation coefficient between typical cable test results and the cable's mechanical parameters are described. Except for the first stage strands and contact points, the third and fourth stages show more influence on the increasing rate of the maximum deformation of the cable. With increasing plastic deformation rate, the Cu strands seem to absorb most of the irreversible plastic strain.

The CWS conductor design with deeper strand indentations seems to go along with more extensive plastic deformation. For the CWS and STP samples tested, it appears that the elastic modulus change rate and the strand indentations of the shorter twist pitch samples are both higher than for both the longer twist pitch samples. However, the E_y of the shorter twist pitch is still higher than that of the longer twist pitch, no matter how the E_y decrease.

The length of the Cu strand twist pitch is about half that of the SC strands in the CWS samples, which could increase the number of strand contact points. However, the STP of the Cu strand probably causes the deeper indentations and subsequent damage of the SC strands. When unraveling the

**Figure 20.** The absolute value of the Pearson correlation coefficient between cable test results and cable mechanical construction properties.

conductor, for the CWS-C01 sample, several broken SC strands were found, meaning that the soft Cu strands are not soft enough to absorb the strong impactations during cable manufacturing. Applying an STP of Cu strand as in the CWS, the diameter of the CWS's first cabling stage will be larger than for the STP samples. When the first stage triplets are twisted into the second stage cable, the plastic deformation of the CWS will be significantly higher than in the STP. In the meantime, the Cu strands in the STP are always in a state of line contact with each other, which could disperse the pressure between first stage cables.

The drawback of higher stiffness seems to be deeper indentation and higher plastic deformation. Excessive indentation may cause irreversible strand performance degradation. Plastic deformation may change the strain distribution in the filaments. In order to maintain acceptable cable stiffness and strand indentations of STP cable, the twist pitch of every stage will be optimized to the average length between STP-S01 and STP-S02. For CWS samples, the twist pitch will further increase by about 10% compared to CWS-C02, in order to decrease the indentations, and retain sufficient cable stiffness. The detailed conductor parameter optimizations are listed in table 5.

Table 5. The optimized conductor design parameters.

| Item | STP-S03 | CWS-C03 |
|----------------------------|--|--------------------|
| Strand diameter | 1.0 ± 0.005 mm | |
| Number of SC strands | 900 Nb ₃ Sn | |
| Number of Cu strands | 522 Cu | |
| Cable layout | [(2 SC + 1 Cu) × 3 × 5 × 5 + core] × 6 | |
| Stage 1 (2 SC + 1 Cu) [mm] | 32.5 ± 2 | SC: 55 ± 3, Cu: 25 |
| Stage 2 (× 3) [mm] | 67 ± 5 | 90 ± 5 |
| Stage 3 (× 5) [mm] | 105 ± 8 | 120 ± 8 |
| Stage 4 (× 5 + core) [mm] | 175 ± 10 | 190 ± 10 |
| Final stage [mm] | 450 ± 20 | 450 ± 20 |
| Core layout | 3 × 4 | |
| Core pitch stage 1 (3 Cu) | 80 ± 5 mm | |
| Core pitch stage 2 (× 4) | 110 ± 10 mm | |
| Sub-wrap | 0.1 × 20 mm | |
| Coverage | 50% | |
| Wrap | 0.1 × 40 mm | |
| Overlap | 30%–40% | |
| Central spiral | 12.5 × 9.5 mm | |
| Cable diameter | 48.5 mm | |
| Conductor dimension | 65 mm | |
| Void fraction [%] | 32.4 | 32 |

6. Conclusion





A detailed and qualitative mechanical structural study has been performed on CFETR TF prototype CICC. The conductors were manufactured following two different cable designs; the STP and the CWS. Both design types were manufactured with two different twist pitch schemes to compare the mechanical properties. The four samples were subjected to transverse mechanical cyclic load testing for 2000 cycles at a peak load of 1200 kN m⁻¹ and 77 K. Furthermore, and cable cross-sectional strand contact point statistics were measured and post mortem strand indentation analysis was carried out. The analysis shows that shorter twist pitch increases the strand contact points per unit length leading to an increase of the cable stiffness but also increasing the indentations of SC strands. The CWS-type conductors show more stiffness than the STP type, but more severe strand indentation damage was found. The conductor design will be further optimized, and the new conductor will be manufactured and tested for current sharing temperature (T_{cs}) and AC loss.

Acknowledgments

This work was supported by the National Key R&D Program of China (Grant No. 2017YFE0301404), the Fund of Natural Science Foundation of China (Grant No. 51677184), and the

Youth Innovation Promotion Association, Chinese Academy of Sciences.

ORCID iDs

Zichuan Guo  <https://orcid.org/0000-0002-0795-6131>
 Jinggang Qin  <https://orcid.org/0000-0002-5652-3447>
 Fang Liu  <https://orcid.org/0000-0002-2027-8080>
 Arend Nijhuis  <https://orcid.org/0000-0002-1600-9451>

References

- [1] Song Y T *et al* 2014 Concept design of CFETR tokamak machine *IEEE Trans. Plasma Sci.* **42** 503–9
- [2] Bruzzone P *et al* 2008 Results of a new generation of ITER TF conductor samples in SULTAN *IEEE Trans. Appl. Supercond.* **18** 459–62
- [3] Clazynski D 2007 Review of Nb₃Sn conductors for ITER *Fusion Eng. Des.* **82** 488–97
- [4] Devred A *et al* 2014 Challenges and status of ITER conductor production *Supercond. Sci. Technol.* **27** 044001
- [5] Muzzi L *et al* 2015 Cable-in-conduit conductors: lessons from the recent past for future developments with low and high temperature superconductors *Supercond. Sci. Technol.* **28** 053001
- [6] Bessette D and Mitchell N 2008 Review of the results of the ITER toroidal field conductor R&D and qualification *IEEE Trans. Appl. Supercond.* **18** 1109–13
- [7] Nijhuis A 2008 A solution for transverse load degradation in ITER Nb₃Sn CICC: verification of cabling effect on Lorentz force response *Supercond. Sci. Technol.* **21** 054011
- [8] Nijhuis A and Ilyin Y 2006 Transverse load optimization in Nb₃Sn CICC design; influence of cabling, void fraction and strand stiffness *Supercond. Sci. Technol.* **19** 945–62
- [9] Mitchell N *et al* 2013 Reversible and irreversible mechanical effects in real cable-in-conduit conductors *Supercond. Sci. Technol.* **26** 114004
- [10] Nabara Y *et al* 2014 Impact of cable twist pitch on T_{cs} -degradation and AC loss in Nb₃Sn conductors for ITER central solenoids *IEEE Trans. Appl. Supercond.* **24** 4200705
- [11] Bajas H *et al* 2012 Approach to heterogeneous strain distribution in cable-in-conduit conductors through finite element simulation *IEEE Trans. Appl. Supercond.* **22** 4803104
- [12] Bajas H, Durville D and Devred A 2012 Finite element modelling of cable-in-conduit conductors *Supercond. Sci. Technol.* **25** 054019
- [13] Durville D 2005 Numerical simulation of entangled materials mechanical properties *J. Mater. Sci.* **40** 5941–8
- [14] Qin J *et al* 2015 Optimization of CFETR CSMC cabling based on numerical modeling and experiments *Supercond. Sci. Technol.* **28** 125008
- [15] Tomone S *et al* 2015 Influence of indentation on the critical current of Nb₃Sn strands *Proc. 25th Int. Cryogenic Engineering Conf. and Int. Cryogenic Materials Conf. 2014* 67 (Physics Procedia) 908–13
- [16] Qin J G *et al* 2016 Impact of indentation on the critical current of Bi2212 round wire *IEEE Trans. Appl. Supercond.* **26** 8401005
- [17] Qin J *et al* 2017 New design of cable-in-conduit conductor for application in future fusion reactors *Supercond. Sci. Technol.* **30** 115012
- [18] Nijhuis A *et al* 2004 Change of interstrand contact resistance and coupling loss in various prototype ITER NbTi

- conductors with transverse loading in the Twente cryogenic cable press up to 40 000 cycles *Cryogenics* **44** 319–39
- [19] Yagotintsev K A *et al* 2019 Overview of verification tests on AC loss, contact resistance and mechanical properties of ITER conductors with transverse loading up to 30 000 cycles *Supercond. Sci. Technol.* **32** 105015
- [20] Sanabria C *et al* 2015 Metallographic autopsies of full-scale ITER prototype cable-in-conduit conductors after full testing in SULTAN: 1. The mechanical role of copper strands in a CICC *Supercond. Sci. Technol.* **28** 085005
- [21] Sanabria C *et al* 2015 Metallographic autopsies of full-scale ITER prototype cable-in-conduit conductors after full cyclic testing in SULTAN: II. Significant reduction of strand movement and strand damage in short twist pitch CICCs *Supercond. Sci. Technol.* **28** 125003
- [22] Sanabria C *et al* 2016 Metallographic autopsies of full-scale ITER prototype cable-in-conduit conductors after full cyclic testing in SULTAN: III. The importance of strand surface roughness in long twist pitch conductors *Supercond. Sci. Technol.* **29** 074002
- [23] Sanabria C *et al* 2012 Evidence that filament fracture occurs in an ITER toroidal field conductor after cyclic Lorentz force loading in SULTAN *Supercond. Sci. Technol.* **25** 075007
- [24] Nijhuis A and Ilyin Y 2009 Transverse cable stiffness and mechanical losses associated with load cycles in ITER Nb₃Sn and NbTi CICCs *Supercond. Sci. Technol.* **22** 055007
- [25] Breschi M *et al* 2012 Results of the TF conductor performance qualification samples for the ITER project *Supercond. Sci. Technol.* **25** 095004
- [26] Liu F *et al* 2018 Indentation effects on strain sensitivity of critical current for internal-tin Nb₃Sn strand *Fusion Eng. Des.* **137** 373–7
- [27] Qin J G *et al* 2016 Cabling technology of Nb₃Sn conductor for CFETR central solenoid model coil *IEEE Trans. Appl. Supercond.* **26** 4801305
- [28] Hyvarinen A and Oja E 2000 Independent component analysis: algorithms and applications *Neural Netw.* **13** 411–30